

ORIGINAL ARTICLE

Open Access



Developing innovative and cost-effective UAS-PPK module for generating high-accuracy digital surface model

Cheng-Hao Lu^{1*} , Shu-Min Tsai², Ming-Tien Wu² and Di-Yi Lin³

Abstract

Traditional indirect georeferencing requires time-consuming and labor-intensive field surveys to obtain ground control points (GCPs), making it challenging to apply in high-risk areas with limited accessibility. This study proposes a novel and low-cost system for direct georeferencing using unmanned aerial system post-processing kinematics (UAS-PPK), which is less than a quarter of the price of commercially available products. To evaluate the accuracy of the aerial surveys of the custom-built module and digital surface models, we used 15 checkpoints (CPs) and 99 validation points (VPs). The results showed that this UAS-PPK module could deliver high-precision aerial surveys with a root mean square error (RMSE) of less than 4 cm for three dimensions without using control points. After adding one GCP, the RMSE of three dimensions was close to that of traditional aerial survey methods using 12 GCPs, having a vertical accuracy of 2.51 cm. The same 99 VPs were used to evaluate the accuracy of the digital surface model produced using UAS-PPK. The results showed that the accuracy was close to that of traditional aerial survey methods, having an average error of less than 3 cm. We demonstrated the self-made attachable UAS-PPK module to be a reliable and accurate survey tool in geoscience applications.

Key Points

1. A novel and low-cost UAS-PPK geomorphic monitoring technology was proposed.
2. After accuracy assessment, this innovative module can achieve cm-level accuracy.
3. This UAS-PPK module could be greatly expanded in geoscience applications, especially in areas that are difficult to access.

Keywords Digital surface model, Geomorphic monitoring, Unmanned aerial system, Post-processing kinematics, Georeferencing

1 Introduction

The demand for generating digital surface models (DSMs) from unmanned aerial systems (UASs) images by structures from motion (SfM) techniques has increased significantly. Many studies have confirmed the effectiveness of these technologies in geoscience research, geomorphic monitoring or environmental management. Moreover, there is an increasing demand for efficient and rapid acquisition of high-resolution, high-precision

*Correspondence:

Cheng-Hao Lu
luch@gms.npu.edu.tw

¹ Department of Tourism and Leisure, National Penghu University of Science and Technology, Penghu County, Taiwan, ROC

² Department of Communication Engineering, National Penghu University of Science and Technology, Penghu County, Taiwan, ROC

³ Department of Civil Engineering, National Kaohsiung University of Science and Technology, Kaohsiung City, Taiwan, ROC



© The Author(s) 2023. **Open Access** This article is licensed under a Creative Commons Attribution 4.0 International License, which permits use, sharing, adaptation, distribution and reproduction in any medium or format, as long as you give appropriate credit to the original author(s) and the source, provide a link to the Creative Commons licence, and indicate if changes were made. The images or other third party material in this article are included in the article's Creative Commons licence, unless indicated otherwise in a credit line to the material. If material is not included in the article's Creative Commons licence and your intended use is not permitted by statutory regulation or exceeds the permitted use, you will need to obtain permission directly from the copyright holder. To view a copy of this licence, visit <http://creativecommons.org/licenses/by/4.0/>.

DSMs. These DSMs serve as datasets for repeated erosion or deposition monitoring or the acquiring of detailed geometric spatial resources. Additionally, the recent rapid development of consumer-grade UASs combined with SfM photogrammetry software provides an efficient tool for 3D reconstruction of the environment (Casella et al. 2016; Gonçalves and Henriques 2015; Gruszczynski et al. 2017)—abbreviated as UAS-SfM. The DSMs and orthoimages produced by UAS-SfM photogrammetry can be used in many geoscience-related studies, including fault rupture investigation and surface deformation (Huang et al. 2018; Lin et al. 2018), beach-dune coastal systems (Bastos et al. 2018; Bon de Sousa et al. 2022; Brunier et al. 2016; Kesavan et al. 2022; Lu and Chyi 2020; Mancini et al. 2013; Taddia et al. 2019), impact assessment of extreme marine events and sea level changes in coastal areas (David and Schlurmann 2020; Scarelli et al. 2017), landslide monitoring (Eker and Aydın 2021; Liu et al. 2015; Lucieer et al. 2013; Peter Tian-Yuan et al. 2019; Tempa et al. 2021; Watanabe et al. 2019), hazards monitoring (Lian et al. 2021), estimation of snow depth (Maier et al. 2022) and changes in glacial melting (Bearzot et al. 2022; Xu et al. 2022), and monitoring the morphology of underwater coral reefs (David et al. 2021). Some of vast space is also difficult to access and are expensive to conduct UAS application with labor-intensive survey, such as rangeland (Rango et al. 2009). The above-mentioned study areas have one thing in common—that is, they are all located in high-risk areas with low accessibility and vast space. Consequently, it can be challenging to implement accurate georeferencing of UAS-SfM photogrammetry.

In general, there are two main approaches for remote sensing data georeferencing—that is, indirect georeferencing and direct georeferencing (Aicardi et al. 2016; Kayitakire et al. 2006; Saponaro et al. 2021). Traditional indirect georeferencing obtains the coordinates of the ground control points (GCPs) using time-consuming and labor-intensive field surveys before importing the data into photogrammetry software. Such methods not only reduce the advantage of contactless UAS-SfM photogrammetry, but also mean that it cannot be applied to construct high-precision DSMs or orthoimages for research related to natural disasters or areas with extremely low accessibility (de Haas et al. 2021; Tomaštk et al. 2019). Conversely, direct georeferencing obtains the precise coordinates and three-dimensional position of each aerial image via the global navigation satellite system (GNSS) using unmanned aerial vehicles (UAVs) to directly construct a high-precision DSM without measuring the GCPs (Nota et al. 2022; Stempfhuber and Buchholz 2011). For example, UAS-RTK or UAS-PPK can be georeferenced using on-board real-time kinematic (RTK)

or post-processing kinematic (PPK) positioning systems to perform GNSS signal calculations with the base station on the ground via radio to obtain aerial image coordinates with centimeter-level accuracy (Forlani et al. 2018). Such a technique could apply UAS-SfM photogrammetry to study areas such as landslides, coastal regions, or remote islands where accessibility is extremely low.

Although there are several types of UAS-RTK or UAS-PPK systems on the market—including the DJI P4RTK and Autel EVO RTK systems (Cledat et al. 2020; Gabrlík et al. 2018; Taddia et al. 2020; Tomaštk et al. 2019)—their prices are so high that the financial risk of losing equipment during aerial surveys in many high-risk areas can become untenable. In particular, UAS-RTK is not only costly, but also requires real-time radio transmission of the GNSS signals. Installing radio transmission equipment on a UAV increases the weight of the drone, consumes more power, reduces battery life, and places constraints on communication. Additionally, the accuracy of UAS-RTK decreases as the drone moves farther away from the base, resulting in increasing error levels (Taddia et al. 2020). Some research also demonstrated the performance of USV-RTK and -PPK measurement (Cledat et al. 2020; Gabrlík et al. 2018; Taddia et al. 2020; Tomaštk et al. 2019). This research proposes a novel low-cost, high-precision self-made UAS-PPK module, which can overcome communication problems (out to a distance of 100 km) and is more power efficient. We verified the accuracy of the DSM produced under different experimental conditions to establish the feasibility and accuracy of future applications and monitoring of earth-science related problems.

2 Methodology

2.1 Instrument description and experiment setup

As discussed, UAS-PPK mapping has many advantages, and can also be used as a backup for the UAS-RTK measurement method. However, the biggest challenge for UAS-PPK mapping is to precisely synchronize the timing of camera triggering and the GNSS recording time, especially for a sealed UAS such as the DJI system.

The self-developed attachable PPK module proposed in this study can be applied to a sealed UAS such as the DJI system, and can also be directly connected to the hot-shoe mount of regular cameras. The trigger timestamp of each photograph can be recorded in the GNSS log file within one microsecond. Using the DJI Phantom 4 drone as an example, our self-developed PPK module can be attached to the LED light below the DJI drone motor using a phototransistor. When the drone takes a photograph, the LED flashes, the phototransistor detects this and sends an electronic signal to the GNSS receiver, and the timestamp is recorded in the log file. The GNSS

module used in this research is the Emlid Reach m+, which has the advantages of small size, weighing less than 35 g, low price, and being integrated with inertial measurement unit data, making it suitable for installation on UAVs and facilitating post-processing operations. The PPK module developed in this research integrates a phototransistor, micro GNSS, and a self-developed circuit board. To reduce signal interference, the GNSS antenna is fixed to a stable metal plate, as shown in Fig. 1a.

Using this module and drone, aerial images are obtained, as well as the three-dimensional coordinates of each image. After the PPK calculations, the precise coordinates of each image can be obtained and entered into the aerial survey software—such as Agisoft’s Photoscan (now known as Metashape)—to produce high-precision orthoimages and DSMs. Additionally, the PPK solution requires the GNSS observations of the base station and a rover station. The Emlid Reach RS base-station receiver is placed in the center of the study area (Fig. 1c), and the GNSS observations are started 30 min before the start of a flight mission and continued for 30 min after the mission ends.

To ascertain the accuracy of the self-developed UAS-PPK system in producing the DSM, three experiments were conducted. The first was a traditional aerial survey, in which 12 GCPs were set up for aerial survey processing (12 GCPs); the second used the PPK method, which did not use any GCPs; the third was the PPK method plus a ground control point (PPK + 1GCP). Figure 2 shows the method and the data processing flow

adopted in this study. The relevant procedural details are described in the following subsections.

2.2 Survey flights

For aerial photography, we used the advanced DJI Phantom 4 drone and obtained image datasets to enable comparison with the above experiment. This study used single-grid automatic flight planning to obtain nadir images with a flight area of 0.1 km², a total of 281 images being obtained. The forward and side overlap ratios for flight planning were set to 80% and 70%, respectively. The flight altitude was approximately 50 m, the ground sampling distance (GSD) was approximately 1.3 cm, and the flight speed was set to 5 m·s⁻¹.

Considering the synchronization problem between the camera trigger and the GPS timestamp record, the drone took photographs in hover and capture mode—that is, the UAV stops at each shooting point for image capturing, which can reduce errors caused by delayed recording. In the future, if a camera with a hot-shoe mount is used, the hover and capture mode need not be used, which should greatly improve the aerial photography efficiency. The GNSS device used in this study—that is, the Emlid Reach m+—could connect the camera shutter via a hot-shoe mount, so each photograph taken could be recorded within one microsecond. Moreover, using the PPK solution, the exact coordinate of each photograph could be determined.



Fig. 1 Images of the research equipment. **a** Self-made UAS-PPK system (components include a self-made circuit board, a GNSS receiver, a phototransistor, and a GNSS antenna); **b** Total station for surveying; **c** PPK base station

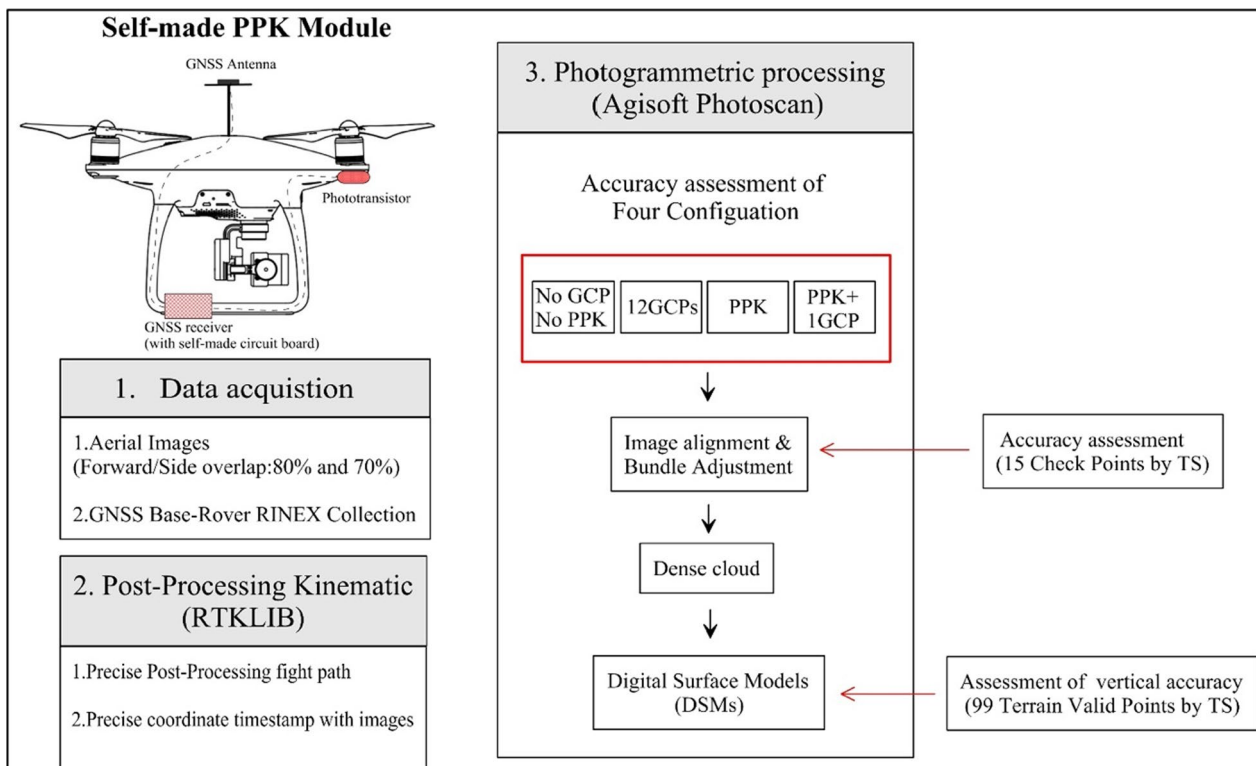


Fig. 2 Research flow chart

2.3 The post-processing kinematic (PPK) process

The PPK process includes two steps—that is, PPK processing and geotagging. As far as the PPK workflow is concerned, accurate coordinates are not calculated in real time, but are obtained using an algorithm, which must operate independently in the field via a base station and a rover, recording raw GNSS observation data in RINEX 3.03 format. The GNSS base station and the rover observation files are then imported into the RTKLIB open-source software for processing. Using the RTKLIB algorithm (Romero-Andrade et al. 2019), the coordinates of the absolute position of the rover station relative to the base station can be determined by calculating the distance between them, commonly known as the baseline.

With the RTKLIB software, it is necessary to first import a RINEX observation file and a navigation file from the base station, and then the RINEX file from the rover. The Kinematic feature is then selected under positioning mode and the three-dimensional coordinate values of the base station are entered. Under antenna type, the delta-U correction value (an offset of 0.25 m from the antenna phase center to the camera center) can be entered. Since the GNSS antenna is installed directly above the camera and the drone flight mode is hover and capture, the effects of E and N can be ignored. Using the delta-U correction value, the coordinates of the center

of each photograph can be adjusted and calculated relative to the antenna phase center. After the calculation is performed, the precise coordinates of each timestamped photograph can be obtained, and the status of each photograph is known—that is, whether it is fixed or floating. Subsequently, the *.pos file can be converted into a *.txt file, which can be read by the photogrammetric software, and the geotagging process can be completed.

2.4 Photogrammetric processing

After all the photographs had been corrected using the PPK procedure and offset correction, Agisoft Metashape—selected as the software of choice for photogrammetry processing—was used to sequentially produce three sets of experimentally designed DSM data for comparison. Photoscan is a software suite designed to achieve 3D reconstruction and to produce DSMs and georeferencing orthoimages. A considerable number of researchers have used this software for geoscience-related research (Javernick et al. 2014; Lucieer et al. 2013; Mancini et al. 2013; Taddia et al. 2020; Warrick et al. 2017; Westoby et al. 2018). This software combines SfM and the SfM-MVS (multiview stereo) algorithms to obtain the position and pose of a sensor from a series of overlapping photographs (Westoby et al. 2018).

Three steps are required to execute this software (Agisoft 2018) for 3D reconstruction. The first step is to import photographs and perform image alignment, after which the image coordinates calculated using PPK are imported. To obtain better results, the parameter accuracy of image alignment can be set to its highest value, the software using the scale invariant feature transform (SIFT) algorithm to automatically detect key points in the image. After the key points have been identified, the camera pose of the camera station and the sparse cloud can be produced through bundle adjustment.

The second step is to convert the sparse cloud into an absolute spatial coordinate system. In this study, we wanted to compare the difference in accuracy between direct and indirect georeferencing. In the indirect georeferencing process, 12 GCPs with known coordinates were used to convert the image to an absolute spatial coordinate system, whereas in the direct georeferencing process, the precise coordinates of the image obtained from the PPK for bundle adjustment were used (Fazeli et al. 2016; Gabrlík et al. 2018). In the experimental setting of the PPK + 1GCP model, the added control point in the center of the study area was used for coordinate transformation. We then entered 15 check points (CPs) into the software to perform the accuracy assessment for the three experimental settings, which used the root mean square error (RMSE) to evaluate the horizontal and vertical accuracy of the model. The formula for the RMSE can be expressed as follows:

$$RMSE_x = \sqrt{\frac{\sum_{i=1}^n (x_{data,i} - x_{check,i})^2}{n}} = \sqrt{\sum_{i=1}^n \Delta x_i^2} \quad (1)$$

$$RMSE_y = \sqrt{\frac{\sum_{i=1}^n (y_{data,i} - y_{check,i})^2}{n}} = \sqrt{\sum_{i=1}^n \Delta y_i^2} \quad (2)$$

$$RMSE_z = \sqrt{\frac{\sum_{i=1}^n (z_{data,i} - z_{check,i})^2}{n}} = \sqrt{\sum_{i=1}^n \Delta z_i^2} \quad (3)$$

where n denotes the number of checkpoints, $x_{data,i}$, $y_{data,i}$, $z_{data,i}$ denote the coordinates and elevation values of checkpoint i in the model, $x_{check,i}$, $y_{check,i}$, $z_{check,i}$ denote the coordinates and elevation values measured by the total station for checkpoint i , and Δx_i , Δy_i , Δz_i denote the differences between the coordinate values of checkpoint i in the x , y , and z directions.

After the accuracy assessment of the CP residual, the difference between the coordinates estimated by

the photogrammetric model and the real coordinates measured by the total station could be determined.

The third step is to produce a dense point cloud and DSM. We set the densification parameter to high and used an aggressive depth filter. The Photoscan software uses an inverse distance weighted algorithm to interpolate the dense point cloud to produce a digital surface. Finally, we used validation points (VPs) to evaluate the accuracy of the DSM.

2.5 Ground validation survey

Before flying, we measured 12 well-distributed GCPs and 15 CPs within the flight range using the Nikon Nivo M+ total station and Trimble R6-4 GNSS, whose localities are shown in Fig. 3. The GCPs were used for georeferencing and the optimization of aerotriangulation in the photogrammetric workflow.

The aim of this paper is to evaluate the accuracy of the self-made, low-cost PPK modules on the DSMs. Ninety-nine VPs were surveyed using the total station throughout the area. These VPs were used to evaluate the vertical accuracy of the DSM produced by the photogrammetric process to establish the terrain accuracy of the traditional aerial survey, the self-made PPK, and the PPK + 1GCP method. We calculated the difference in elevation between the DSM and the total station measurement for the three experimental setups from each validation site ($DH = HTS - HDSM$, where DH is the difference of height; HTS is the height which is measured by Total Station; $HDSM$ is the height derived from DSM). We then evaluated the distributions of elevation differences by means of frequency distribution histograms and regression analyses and calculated the mean and standard deviation.

3 Results

3.1 Accuracy assessment of check points of different UAS photogrammetry methods

Figure 4 shows a comparison of the results of the average RMSE of four different aerial survey methods at 15 checkpoints. Figure 4a includes the accuracy assessment without CPs and VPs and shows that the horizontal RMSE is of the order of tens of centimeters, and the vertical RMSE is 29.63 m. Figure 4b compares the three different aerial survey methods—that is, the 12GCPs, PPK, and PPK + 1GCP methods. With a GSD of 1.3 cm, the RMSEs of X , Y , and Z for the 12GCPs method are 3.63, 2.99, and 2.45 cm, respectively. The RMSEs of X , Y , and Z for the PPK method are 3.64, 3.58, and 3.32 cm, respectively. The RMSEs of X , Y , and Z for the PPK + 1GCP method are 3.75, 3.52, and 2.51 cm, respectively.

From these results, it is evident that although the traditional aerial survey method (12GCPs) has the best



Fig. 3 Experimental flight field map. The red triangles are the 12 GCPs; the green triangles are the 15 CPs; the yellow circles are the terrain VPs

accuracy, the horizontal accuracy of the other methods reaches 2–3 GSD and the vertical accuracy is approximately 1.9 GSD. However, the low-cost PPK aerial survey method developed in this study (without the use of GCPs) has an accuracy quite close to that of the 12GCPs method, but the vertical accuracy (approximately 2.6 GSD) is slightly worse. When the PPK method adds one GCP, its overall precision is close to that of the traditional aerial survey method, especially the vertical accuracy, which is also approximately 1.9 GSD. This accuracy, without the need for multiple GCPs, can be used for high-precision monitoring in many geoscience applications.

3.2 DSM accuracy assessment

To evaluate the absolute accuracy of the DSMs produced by the three aerial survey methods, as mentioned in Sect. 2.5, we measured two sections in different directions using the total station in the research area, obtaining a total of 99 terrain VPs. We imported these 99 terrain VPs into ArcGIS software and used the extraction tool in Arctoolbox to extract the elevation values at the same 99 positions from the DSM produced by the three aerial survey methods. A statistical analysis of the elevation difference between the VP measured by the total station and the same point of the corresponding DSM

was then conducted. This comparison could be affected by how the DSM interpolation is achieved as well as the elevation interpolation during software sampling. The interpolation method used by the Metashape software is the inverse distance weighted algorithm. This effect could be more obvious where the point cloud is sparse and the volume of data is small.

Table 1 summarizes the vertical DSM error statistics for the three aerial survey methods. The average error for the PPK method is similar to that of the 12GCPs method, approximately 2.1 GSD (which matches the previous VP RMSE), but the error for the PPK + 1 method is approximately 3 GSD. Nonetheless, the standard deviations, maximum values, and minimum values for the three aerial survey methods are very close. It is worth noting that the minimum errors of the three survey methods are between -13.7 and -17.5 cm—that is, approximately 10 to 13 GSDs. The reasons for this are analyzed in the discussion section.

To further verify the accuracy of the DSMs produced by the three aerial survey methods, this study used the absolute errors of the 99 VPs for frequency distribution calculations, as shown in the upper graphs of Fig. 5. The histograms from the three methods show that the errors are closely clustered. The 12GCPs method is the most

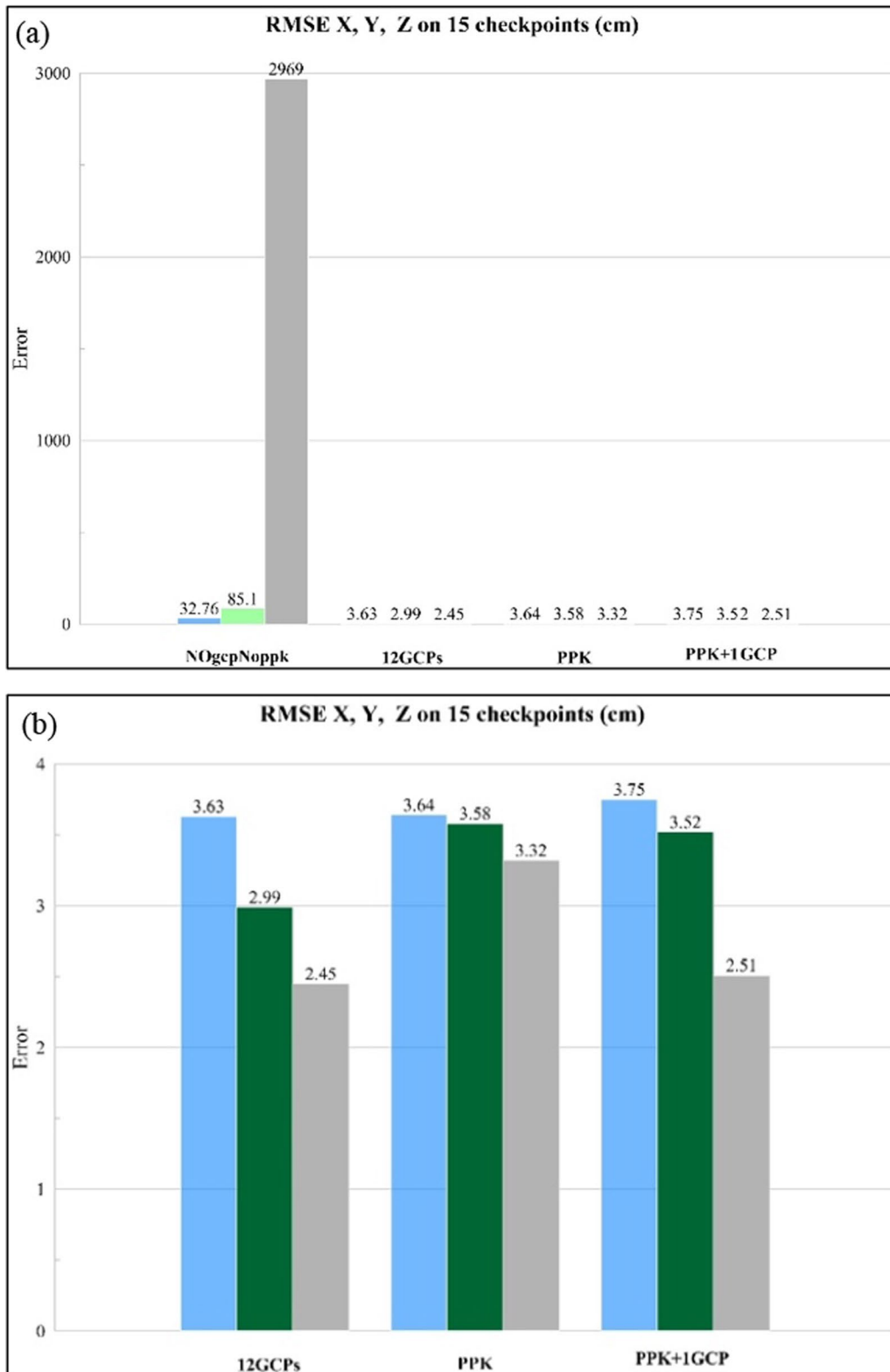


Fig. 4 **a** Comparison of the VP accuracy of the four aerial survey methods (including those without CPs and VPs). **b** Enlarged comparison of the VP accuracy of the three methods

Table 1 DSM elevation error statistics for the three aerial survey methods (cm)

	12GCPs	PPK	PPK + 1GCP
Average Error	-2.73	-2.57	-3.91
Standard Deviation	5.24	5.40	5.40
Max	5.35	5.55	4.53
Min	-13.67	-16.30	-17.46

concentrated, followed by the PPK + 1 method, and then the PPK method. The overall elevation error is within 10 to -15 cm.

The lower part of Fig. 5 shows the regression analysis of the elevations of the three aerial survey methods and the elevation values measured by the total station. The slopes of the linear regression lines for all three methods are close to 1—that is, the measured values correspond well with the true values obtained from the total station—and all correlation coefficients (R^2 values) are above 0.99 (P -values < 0.0001). Moreover, the data points lie close to the regression lines. This means that the UAS-PPK system developed in this study is stable and yields highly accurate DSMs.

4 Discussion

4.1 Accuracy of the self-developed UAS-PPK system compared with traditional aerial survey methods

Implementing high-accuracy UAS-SfM photogrammetry with no GCPs, or only a small number of GCPs, could be an efficient, risk-reduced telemetry method. However, whether its accuracy can reach the level of traditional UAS-SfM methods needs to be evaluated. This study proposed a low-cost, high-precision UAS-PPK system and compared its accuracy with that of traditional aerial survey methods by means of in-field verification.

In terms of the horizontal RMSE, of the traditional aerial survey method the 12GCPs method yields the best results, with errors in X and Y of 2.8 GSD and 2.2 GSD, respectively. The UAS-PPK system developed in this study yields similar results, with errors in X and Y of 2.8 GSD and 2.8 GSD, respectively. When a GCP is added to the PPK method, the X error is 2.9 GSD and the Y error drops to 2.7 GSD. The above results show that performance of the self-developed UAS-PPK system is close to that of the traditional aerial survey method in terms of horizontal error.

In terms of the vertical RMSE, the 12GCPs method is also the best, with an error of approximately 1.9 GSD. When the UAS-PPK system has no GCP, the vertical error is approximately 2.6 GSD, and when a GCP is added, the vertical error of the PPK + 1GCP method

drops to 1.9 GSD, which is close to that if the traditional aerial survey methods.

4.2 The accuracy of DSMs derived from the self-made UAS-PPK photogrammetry module

From the DSM accuracy verification tests, it is evident that the absolute negative error of the three aerial survey methods reaches 10–13 GSDs. To understand the spatial distribution of these extreme negative values, we performed a cross-section analysis. Figure 6 shows two terrain profiles plotting elevation versus distance, which compare the elevations of the VPs of the three aerial survey methods with those determined using the total station. From the analysis, it is evident that the topographic profiles of the three aerial survey methods are consistent with the profiles of the total station. However, in the central region (which is covered by grass), the profile for the total station is slightly lower than those of the three aerial surveys. With the exception of the grass-covered area, the rest of the research area is concreted ground or polyurethane (PU) runway, and the four section profiles are almost the same.

Consequently, we classified the ground surface in the research area into three types—that is, concreted areas, grassed areas, and PU runways—for comparison of the elevation errors. The results are presented in Table 2. The average error in the grassed area is the largest, reaching -6.75 to -8.6 cm, which is approximately 5–7 GSDs; the average errors in concreted areas and PU runways are similar (between 1.86 and -0.09 cm, which is approximately 1–2 GSD). This result matches the observation of the profile analysis. We also compared the elevation error between different terrains by categorizing the terrain of the research area as level or sloping. The results are shown in Table 3. The difference in elevation error between these two terrain types is approximately 1–2 GSD, which is small. The reason for the errors in the three aerial survey methods being larger in the grassed area compared with the concreted areas and PU runways may be due to differences in the measurement methods and tools used to determine the ground elevation. The total station method measures elevation by determining heights using a surveying pole placed on the ground surface, while aerial surveys calculate the height of the terrain surface by means of image processing. In areas with vegetation, the height of the vegetation surface is calculated instead of the ground. Consequently, the taller the vegetation, the greater the elevation difference. Another possible reason for the discrepancy is that it may be difficult to extract sufficient corresponding feature points for SfM algorithms on relatively homogeneous ground

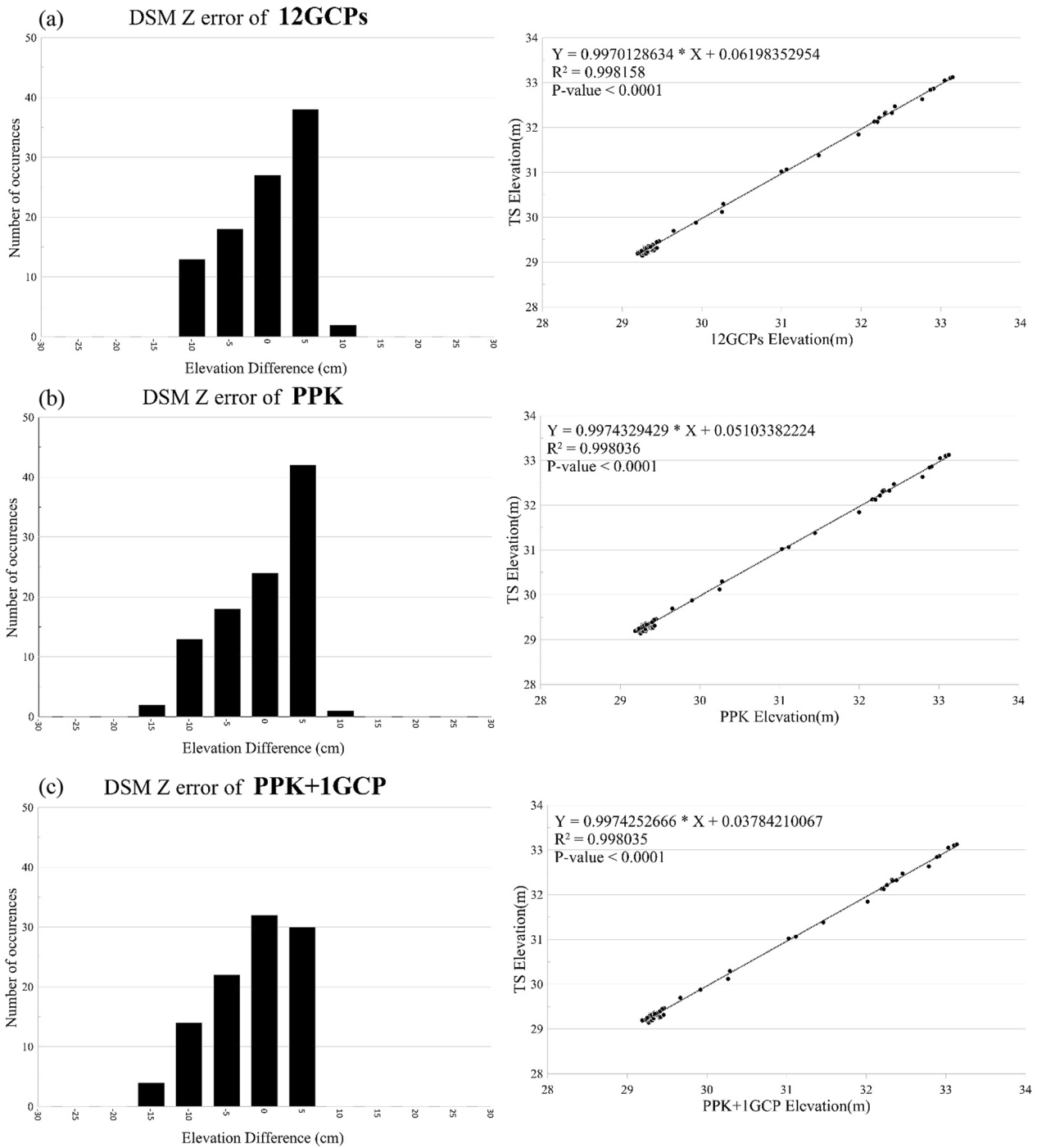


Fig. 5 Comparison between elevations of VPs surveyed by the total station and corresponding points extracted from the DSMs. The frequency histogram and linear regression diagram of the elevation difference between DSM and VP of **(a)** 12GCPs, **(b)** PPK, and **(c)** PPK+ 1GCP

surfaces such as grassed areas (Fonstad et al. 2013; Fonstad and Marcus 2010; Forlani et al. 2018; Mancini et al. 2013). For these reasons, the average errors in the

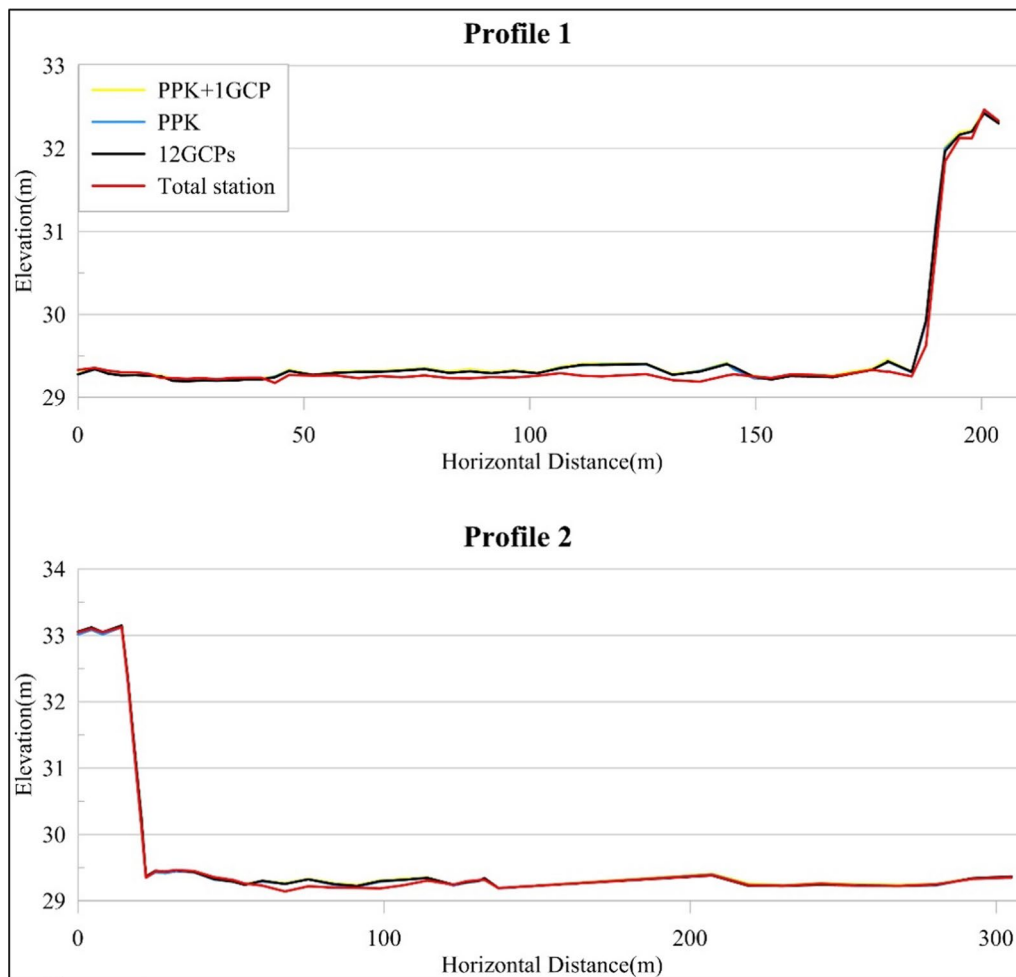


Fig. 6 Plots of the validation points for the three aerial survey methods on two topographic profiles compared with topographic profiles determined by the total station

Table 2 The average elevation error (cm) of the DSM of the three aerial survey methods for different ground covers

	12GCPs	PPK	PPK + 1GCP
Concrete Pavement (n=14)	0.13	1.86	0.25
Grassed Area (n=47)	-6.75	-6.84	-8.16
PU Runway (n=37)	1.29	1.17	-0.09

Table 3 The average error value (cm) of the DSM of the three aerial survey methods for different ground inclinations

	12GCPs	PPK	PPK + 1GCP
Flat (n=80)	-2.46	-2.14	-3.53
Sloping (n=18)	-3.94	-4.50	-5.64

grassed area of the three aerial survey methods are all higher.

5 Conclusions

Our self-developed UAS-PPK system has the advantages of low price, compactness, and high accuracy, unlike the UAS-RTK system, which is limited by radio communications, reduced endurance, and increased errors when the drone is far from the base station. The attachable PPK module integrates phototransistors, a micro global navigation satellite system (GNSS), and a custom circuit board. It can be applied to a sealed UAS and can be directly connected to a camera hot shoe on ordinary UAVs to record the time in the GNSS log file within a microsecond of the camera shutter being triggered. Using the PPK method, the precise coordinates of each image can be obtained.

15 check points were used to evaluate the RMSE of the traditional aerial survey methods—that is, using 12 GCPs (denoted as 12GCPs), PPK without a GCP (denoted as PPK), and PPK with one GCP (PPK + 1GCP). The results showed that the self-developed UAS-PPK system exhibited RMSEs for all three axes within 4 cm when no check-points (CPs) were used, slightly higher than the 12GCPs of the traditional aerial survey method. When a CP was added to the UAS-PPK module, its three dimensions RMSE was close to the traditional aerial survey method. Furthermore, to evaluate the accuracy of the DSM produced by the three aerial survey methods, we measured 99 terrain VPs to assess elevation accuracy. The results showed that the accuracy of UAS-PPK module was close to that of traditional aerial surveys, the average error being within 3 cm, although we found that larger errors occurred in vegetated areas.

The above accuracy verification results demonstrated that the self-developed attachable UAS-PPK module is a promising measurement tool and that the precision of the DSMs produced by the system is less than 2 cm. Coupled with its advantages of low price and long flying distance, the application of such UAVs in related research could be greatly expanded, especially in areas that are difficult to reach.

Acknowledgements

The authors are grateful to the editor and two anonymous reviewer for their valuable comments and suggestion that greatly improved this manuscript. The survey help from Yi-Quan Zeng is deeply appreciated.

Author contributions

C-HL and D-YL plan and performed the conceptualization and validation experiment. S-MT and M-DW designed and built the PPK module and optimization. All authors contributed to scientific discussion, module design, methodologies improvement and writing. All authors read and approved the final manuscript.

Funding

This study was supported by National Science and Technology Council, Taiwan, R.O.C. [Grant number 110-2116-M-346-001-MY2 (C.-H. Lu) and 109-2119-M-001-011].

Data availability

The datasets that support the findings of this study are available from the corresponding author on reasonable request.

Declarations

Competing interests

The authors declare no conflict of interest.

Received: 7 July 2023 Accepted: 1 November 2023

Published online: 20 November 2023

References

Agisoft (2018) Agisoft photoscan user manual: professional edition. Version 1.4

- Aicardi I, Nex F, Gerke M, Lingua AM (2016) An image-based approach for the co-registration of multi-temporal UAV image datasets. *Remote Sens.* <https://doi.org/10.3390/rs8090779>
- Bastos A, Ponte Lira C, Calvão J, Catalao J, Andrade C, Pereira AJ, Taborá R, Rato D, Pinho P, Correia O (2018) UAV derived information applied to the study of slow-changing morphology in dune systems. *J Coast Res.* <https://doi.org/10.2112/S185-046.1>
- Bearzot F, Garzonio R, Di Mauro B, Colombo R, Cremonese E, Crosta GB, Delaloye R, Hauck C, Morra Di Cella U, Pogliotti P, Frattini P, Rossini M (2022) Kinematics of an Alpine rock glacier from multi-temporal UAV surveys and GNSS data. *Geomorphology* 402:108116. <https://doi.org/10.1016/j.geomorph.2022.108116>
- Bon de Sousa L, Costas S, Ferreira Ó (2022) Effect of survey parameters on unmanned aerial vehicles-derived topography for coastal dune monitoring. *J Appl Remote Sens* 16(3):034513
- Brunier J, Fleury J, Anthony EJ, Gardel A, Dussouillez P (2016) Close-range airborne Structure-from-Motion Photogrammetry for high-resolution beach morphometric surveys: examples from an embayed rotating beach. *Geomorphology* 261:76–88. <https://doi.org/10.1016/j.geomorph.2016.02.025>
- Casella E, Rovere A, Pedroncini A, Stark CP, Casella M, Ferrari M, Firpo M (2016) Drones as tools for monitoring beach topography changes in the Ligurian Sea (NW Mediterranean). *Geo-Mar Lett* 36(2):151–163. <https://doi.org/10.1007/s00367-016-0435-9>
- Cledat E, Jospin LV, Cucci DA, Skaloud J (2020) Mapping quality prediction for RTK/PPK-equipped micro-drones operating in complex natural environment. *ISPRS J Photogramm Remote Sens* 167:24–38. <https://doi.org/10.1016/j.isprsjprs.2020.05.015>
- David CG, Schlurmann T (2020) Hydrodynamic drivers and morphological responses on small coral islands—the thoondu spit on Fuvahmulah, the Maldives. *Front Mar Sci.* <https://doi.org/10.3389/fmars.2020.538675>
- David CG, Kohl N, Casella E, Rovere A, Ballesteros P, Schlurmann T (2021) Structure-from-Motion on shallow reefs and beaches: potential and limitations of consumer-grade drones to reconstruct topography and bathymetry. *Coral Reefs* 40(3):835–851. <https://doi.org/10.1007/s00338-021-02088-9>
- de Haas T, Nijland W, McArdell BW, Kalthof MWML (2021) Case report: optimization of topographic change detection with UAV structure-from-motion photogrammetry through survey co-alignment. *Front Remote Sens.* <https://doi.org/10.3389/frsen.2021.626810>
- Eker R, Aydin A (2021) Long-term retrospective investigation of a large, deep-seated, and slow-moving landslide using InSAR time series, historical aerial photographs, and UAV data: the case of Devrek landslide (NW Turkey). *CATENA* 196:104895. <https://doi.org/10.1016/j.catena.2020.104895>
- Fazeli H, Samadzadegan F, Dadrass Javan F (2016) Evaluating the potential of RTK-UAV for automatic point cloud generation in 3D rapid mapping. *Int Arch Photogramm Remote Sens Spat Inf Sci.* <https://doi.org/10.5194/isprsarchives-XLI-B6-221-2016>
- Fonstad MA, Marcus WA (2010) High resolution, basin extent observations and implications for understanding river form and process. *Earth Surf Process Landf* 35(6):680–698. <https://doi.org/10.1002/esp.1969>
- Fonstad MA, Dietrich JT, Courville BC, Jensen JL, Carbonneau PE (2013) Topographic structure from motion: a new development in photogrammetric measurement. *Earth Surf Process Landf* 38(4):421–430. <https://doi.org/10.1002/esp.3366>
- Forlani G, Dall'Asta E, Diotri F, Cella UMD, Roncella R, Santise M (2018) Quality assessment of DSMs produced from UAV flights georeferenced with on-board RTK positioning. *Remote Sens.* <https://doi.org/10.3390/rs10020311>
- Gabrlík P, la Cour-Harbo A, Kocmanova P, Zalud L, Janata P (2018) Calibration and accuracy assessment in a direct georeferencing system for UAS photogrammetry. *Int J Remote Sens* 39:1–29. <https://doi.org/10.1080/01431161.2018.1434331>
- Gonçalves JA, Henriques R (2015) UAV photogrammetry for topographic monitoring of coastal areas. *ISPRS J Photogramm Remote Sens* 104:101–111. <https://doi.org/10.1016/j.isprsjprs.2015.02.009>
- Gruszczynski W, Matwij W, Cwiakala P (2017) Comparison of low-altitude UAV photogrammetry with terrestrial laser scanning as data-source methods for terrain covered in low vegetation. *ISPRS J Photogramm Remote Sens* 126:168–179. <https://doi.org/10.1016/j.isprsjprs.2017.02.015>
- Huang S-Y, Yen J-Y, Wu B-L, Yen IC, Chuang R (2019) Investigating the Milun Fault: the coseismic surface rupture zone of the 2018/02/06 ML 6.2

- Hualien earthquake, Taiwan. *Terr Atmos Ocean Sci.* <https://doi.org/10.3319/TAO.2018.12.09.03>
- Javernick L, Brasington J, Caruso B (2014) Modeling the topography of shallow braided rivers using Structure-from-Motion photogrammetry. *Geomorphology* 213:166–182. <https://doi.org/10.1016/j.geomorph.2014.01.006>
- Kayitakire F, Hamel C, Defourny P (2006) Retrieving forest structure variables based on image texture analysis and IKONOS-2 imagery. *Remote Sens Environ* 102(3):390–401. <https://doi.org/10.1016/j.rse.2006.02.022>
- Kesavan P, Nagarajan S, De Witt P (2022) Data-driven approach for 2D shoreline, and 3D volumetric change detection analysis: a case study for Jupiter inlet lighthouse outstanding natural area. *J Appl Remote Sens* 16(3):034509
- Lian X, Liu X, Ge L, Hu H, Du Z, Wu Y (2021) Time-series unmanned aerial vehicle photogrammetry monitoring method without ground control points to measure mining subsidence. *J Appl Remote Sens* 15(2):024505
- Lin Y-S, Chuang RY, Yen J-Y, Chen Y-C, Kuo Y-T, Wu B-L, Huang S-Y, Yang C-J (2018) Mapping surface breakages of the 2018 Hualien earthquake by using UAS photogrammetry. *Terr Atmos Ocean Sci.* <https://doi.org/10.3319/TAO.2018.12.09.02>
- Liu C-C, Chen P-L, Matsuo T, Chen C-Y (2015) Rapidly responding to landslides and debris flow events using a low-cost unmanned aerial vehicle. *J Appl Remote Sens* 9(1):096016
- Lu C-H, Chyi S-J (2020) Using UAV-SfM to monitor the dynamic evolution of a beach on Penghu Islands. *Terr Atmos Ocean Sci* 31:283–293. <https://doi.org/10.3319/TAO.2019.09.25.01>
- Lucieer A, Jong SMD, Turner D (2013) Mapping landslide displacements using Structure from Motion (SfM) and image correlation of multi-temporal UAV photography. *Prog Phys Geogr* 38(1):97–116. <https://doi.org/10.1177/0309133313515293>
- Maier K, Nascetti A, van Pelt W, Rosqvist G (2022) Direct photogrammetry with multispectral imagery for UAV-based snow depth estimation. *ISPRS J Photogramm Remote Sens* 186:1–18. <https://doi.org/10.1016/j.isprsjprs.2022.01.020>
- Mancini F, Dubbini M, Gattelli M, Stecchi F, Fabbri S, Gabbianelli G (2013) Using unmanned aerial vehicles (UAV) for high-resolution reconstruction of topography: the structure from motion approach on coastal environments. *Remote Sens.* <https://doi.org/10.3390/rs5126880>
- Nota EW, Nijland W, de Haas T (2022) Improving UAV-SfM time-series accuracy by co-alignment and contributions of ground control or RTK positioning. *Int J Appl Earth Obs Geoinf* 109:102772. <https://doi.org/10.1016/j.jag.2022.102772>
- Peter T-Y, Wang H, Kuo-Wei L, Liao J-J, Pan Y-W (2019) Landslide monitoring with interferometric SAR in Liugui, a vegetated area. *TAO Terr Atmos Ocean Sci* 30(4):5–530. <https://doi.org/10.3319/TAO.2019.04.13.01>
- Rango A, Laliberte A, Herrick J, Winters C, Havstad K, Steele C, Browning D (2009) Unmanned aerial vehicle-based remote sensing for rangeland assessment, monitoring, and management. *J Appl Remote Sens* 3(1):033542
- Romero-Andrade R, Zamora-Maciel A, Uriarte-Adrián JDJ, Pivot F, Trejo-Soto ME (2019) Comparative analysis of precise point positioning processing technique with GPS low-cost in different technologies with academic software. *Measurement* 136:337–344. <https://doi.org/10.1016/j.measurement.2018.12.100>
- Saponaro M, Capolupo A, Caporusso G, Tarantino E (2021) Influence of co-alignment procedures on the co-registration accuracy of multi-epoch SfM points clouds. *Int Arch Photogramm Remote Sens Spatial Inf Sci.* <https://doi.org/10.5194/isprs-archives-XLIII-B2-2021-231-2021>
- Scarelli FM, Sistilli F, Fabbri S, Cantelli L, Barboza EG, Gabbianelli G (2017) Seasonal dune and beach monitoring using photogrammetry from UAV surveys to apply in the ICZM on the Ravenna coast (Emilia-Romagna, Italy). *Remote Sens Appl Soc Environ* 7:27–39. <https://doi.org/10.1016/j.rsase.2017.06.003>
- Stempfhuber W, Buchholz M (2011) A precise, low-cost RTK GNSS system for UAV applications. *Proc. of Unmanned Aerial Vehicle in Geomatics, ISPRS*
- Taddia Y, Corbau C, Zambello E, Pellegrinelli A (2019) UAVs for structure-from-motion coastal monitoring: a case study to assess the evolution of embryo dunes over a two-year time frame in the Po River Delta, Italy. *Sensors.* <https://doi.org/10.3390/s19071717>
- Taddia Y, Stecchi F, Pellegrinelli A (2020) Coastal mapping using DJI phantom 4 RTK in post-processing kinematic mode. *Drones.* <https://doi.org/10.3390/drones4020009>
- Tempa K, Peljor K, Wangdi S, Ghalley R, Jamtsho K, Ghalley S, Pradhan P (2021) UAV technique to localize landslide susceptibility and mitigation proposal: a case of Rinchending Goenpa landslide in Bhutan. *Nat Resour Res* 1(4):171–186. <https://doi.org/10.1016/j.nhres.2021.09.001>
- Tomašič J, Mokroš M, Surový P, Grznárová A, Merganič J (2019) UAV RTK/PPK method—an optimal solution for mapping inaccessible forested areas? *Remote Sens.* <https://doi.org/10.3390/rs11060721>
- Warrick J, Ritchie A, Adelman G, Adelman K, Limber PW (2017) New techniques to measure cliff change from historical oblique aerial photographs and structure-from-motion photogrammetry. *J Coast Res* 33(1):39–55. <https://doi.org/10.2112/JCOASTRES-D-16-00095.1>
- Watanabe J-I, Shao Y, Miura N (2019) Underwater and airborne monitoring of marine ecosystems and debris. *J Appl Remote Sens* 13(4):044509
- Westoby MJ, Lim M, Hogg M, Pound MJ, Dunlop L, Woodward J (2018) Cost-effective erosion monitoring of coastal cliffs. *Coast Eng* 138:152–164. <https://doi.org/10.1016/j.coastaleng.2018.04.008>
- Xu S, Fu P, Quincey D, Feng M, Marsh S, Liu Q (2022) UAV-based geomorphological evolution of the Terminus Area of the Hailuoguo Glacier, Southeastern Tibetan Plateau between 2017 and 2020. *Geomorphology* 411:108293. <https://doi.org/10.1016/j.geomorph.2022.108293>

Publisher's Note

Springer Nature remains neutral with regard to jurisdictional claims in published maps and institutional affiliations.

Submit your manuscript to a SpringerOpen® journal and benefit from:

- Convenient online submission
- Rigorous peer review
- Open access: articles freely available online
- High visibility within the field
- Retaining the copyright to your article

Submit your next manuscript at ► [springeropen.com](https://www.springeropen.com)